LETTER

Thermal Analysis of the Exothermic Reaction between Galvanic Porous Silicon and Sodium Perchlorate

Collin R. Becker,[†,‡] Luke J. Currano,[‡] Wayne A. Churaman,[‡] and Conrad R. Stoldt*[,†]

Department of Mechanical Engineering, University of Colorado, Boulder, Colorado 80309, United States, and U.S. Army Research Laboratory, Adelphi, Maryland 20783, United States

ABSTRACT Porous silicon (PS) films up to ~150 μm thick with specific surface area similar to 700 m^2/g and pore diameters similar to 3 nm are fabricated using a galvanic corrosion etching mechanism that does not require a power supply. After fabrication, the pores are impregnated with the strong oxidizer sodium perchlorate ($NaClO_4$) to create a composite that constitutes a highly energetic system capable of explosion. Using bomb calorimetry, the heat of reaction is determined to be 9.9 ± 1.8 and 27.3 ± 3.2 kJ/g of PS when ignited under N_2 and O_2, respectively. Differential scanning calorimetry (DSC) reveals that the energy output is dependent on the hydrogen termination of the PS.

KEYWORDS: porous silicon • nanoenergetics • calorimetry • MEMS

Porous silicon (PS) is a widely studied material fabricated by electrochemically etching a silicon (Si) wafer to produce a porous structure that can have a thickness of a few nanometers to hundreds of micrometers (1). When the pores of PS are loaded with any one of a number of oxidizers, PS can function as a highly energetic material (2, 3). After loading with oxidizer, the PS-oxidizer composite is typically stable until triggered by a mechanical impact, spark, or heating. Upon one of these stimuli, the composite demonstrates an exothermic reaction ranging from an explosion traveling several kilometers per second that produces a bright flash, a loud audible report, a shattered silicon (Si) substrate, and a significant pressure rise from gas evolution to a less powerful burning of the material traveling only centimeters per second that does not shatter the Si substrate. PS has the advantage of being monolithically integrated into a Si chip and fabricated alongside traditional Si microelectronics and MEMS (4). With the success of achieving an on-chip energetic material, there is interest in fine-tuning PS to serve in applications that demand on-chip power, fuzing, propulsion, or heat. However, the reaction mechanism for energetic PS is not well understood and there is very limited data regarding the heat of reaction, ignition temperature, velocity, or pressure rise of the PS explosive reaction.

In this letter, an explosive composite of PS and sodium perchlorate ($NaClO_4$) is investigated. The PS is fabricated using a galvanic corrosion technique in which thick (up to ~150 μm) films are prepared without the requirement of a power supply, an approach well-suited for Microsystems batch processing. In a method similar to prior work in the literature (3, 5, 6), a solution of $NaClO_4$ in methanol (MeOH) is drop cast on the material to fill the pores in the PS and functions as the oxidizer. The composite is stabilized from oxidation by the hydrogen termination of the internal PS surface area as a FT-IR spectroscopic analysis demonstrates. The extent of the reaction is observed with bomb calorimetry in nitrogen (N_2) and oxygen (O_2) atmospheres. Without the supplementary O_2 environment, the heat of reaction is measured to be 9.9 ± 1.8 kJ/g, but with supplementary O_2 the reaction yields 27.3 ± 3.2 kJ/g and approaches the theoretical value of 33.0 kJ/g for complete Si oxidation by $NaClO_4$.

As a complementary technique to bomb calorimetry, DSC is used to heat the entire sample at a slow rate so that information regarding events prior to explosion is revealed. Results indicate that PS catalyzes complete $NaClO_4$ decomposition once the hydrogen termination has been removed; these surface hydrides desorb from the PS surface at temperatures above approximately 450 °C. If decomposition is triggered locally, i.e. the global network of pores still retains hydrogen termination, an explosion is produced. This is evidenced by a shattered Si substrate and a dent in the copper seal of the stainless steel high pressure DSC pan resulting from high-pressure gas evolution. However, if hydrogen termination has been completely removed from the PS, heat is evolved from Si oxidation but no explosion is observed. Additionally, little to no gas production occurs as even aluminum DSC sample pans not intended to withstand pressure are undamaged. These results demonstrate the important role hydrogen plays in the exothermic reaction of PS with $NaClO_4$.

* To whom correspondence should be addressed. E-mail: conrad.stoldt@colorado.edu.
Received for review October 10, 2010 and accepted November 1, 2010
† University of Colorado.
‡ U.S. Army Research Laboratory.
DOI: 10.1021/am100975u
2010 American Chemical Society

Traditional PS formation requires electrical connection to a Si chip immersed in a hydrofluoric (HF) acid-based electrolyte (1). The Si is biased to promote holes to the semiconductor-electrolyte interface, which serve to oxidize Si atoms and etch the wafer according to eqs 1 and 2 (7).

$$Si + 2h^{+} + 2H^{+} \rightarrow Si^{4+} + H_2 \qquad (1)$$

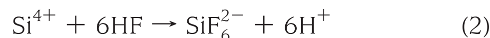

$$Si^{4+} + 6HF \rightarrow SiF_6^{2-} + 6H^{+} \qquad (2)$$

However, in the presence of a chemical oxidant such as dissolved oxygen or hydrogen peroxide (H_2O_2), a noble metal such as platinum or gold can be directly deposited on Si to serve as a cathode while the Si acts as the anode to form a galvanic cell that enables Si etching without requiring an external current source (7−13). The reaction is cathode limited, and by varying the surface area ratio (SAR) of metal to Si, we can control the current (10, 13). Additionally, the choice of electrolyte composition, oxidizing agent, noble metal, Si resistivity, Si dopant type (p- or n-type), and reaction conditions such as stirring control the morphology of the material. Here, platinum (Pt) serves as the cathode and H_2O_2 as the oxidizing agent on P-type Si wafers with a resistivity of 1−20 Ω cm.

Thin film adhesion of Pt to Si is critical for the galvanic mechanism. Without robust Pt adhesion, the HF-based electrolyte will attack any oxide underlying the Pt film, remove the Pt, and inhibit PS formation. Here, Pt deposition is achieved by performing a sputter etch to remove any native oxide (alternatively, a two minute immersion in 10:1 buffered oxide etchant with surfactant (JT Baker; 50% (by volume) ammonium fluoride, 5% HF, ~45% water, ~0.2% surfactant)) followed by sputtering of a 170 nm thick Pt film directly on the Si wafer. Subsequently, a 350 °C anneal for two minutes promotes formation of a platinum silicide, which enhances electrical connectivity to the Si substrate (14). With this method, an increase in etch rate and improved PS structural stability to previous reports of galvanic PS are achieved. The wafer can be etched in HF-based electrolytes for up to 60 min with minimal degradation to the Pt layer and at a high etch rate (~2 μm/min) with only the backside of the Si wafer coated with Pt (1:1 SAR).

Figure 1 shows scanning electron microscope (SEM) images of the cross sections of PS formed on Si wafers with a 1:1 SAR after an (a) 30 min and (b) 60 min galvanic etch in an HF-based electrolyte. The electrolyte is a 3:1 by volume solution of 49% HF in water and ethanol (EtOH) respectively with 2.4% by volume composed of 30% H_2O_2 in water. Mildly stirring the solution both increases the etch rate and improves uniformity of the PS layer across the Si wafer.

For thermal analysis, Si samples approximately 3 cm by 3 cm were etched for 30 or 60 min under the same conditions as in Figure 1. The porosity was measured gravimetrically as 62−65 and 68−69%, respectively. Gas adsorption analysis by the BET (15−18) method finds the pore sizes to be 2.65−2.70 and 2.90−3.05 nm and surface areas of approximately 680 and 710 m^2/g for the 30 and 60 min samples, respectively. The mass of the PS layer was determined by an indirect gravimetric technique. In this method, the calorimeter sample is fractured into several parts. One part is used for calorimetry while the PS mass is measured using a destructive gravimetric technique (1) with the remaining parts. The mass of PS per mass of PS plus Si substrate is calculated and assumed to hold for the sample in the calorimeter.

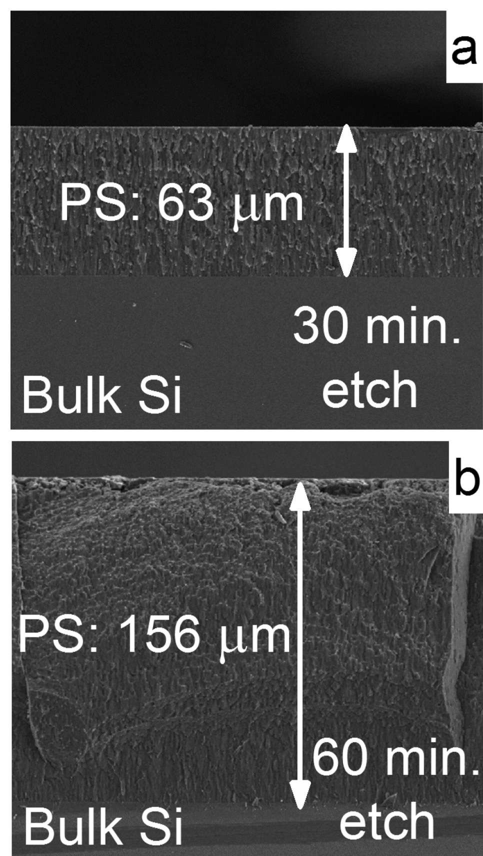

FIGURE 1. SEM images of cross-sections of PS formed after (a) 30 min and (b) 60 min etch.

The PS-$NaClO_4$ energetic material is prepared by drop-casting a 3.2 M $NaClO_4$ (anhydrous) in MeOH solution onto the PS chip and drying for at least 15 min in a nitrogen (N_2) filled glovebox. During drop-casting the solution is dispensed from a syringe such that a thin layer of liquid covers the PS. Upon drying, small white crystals of $NaClO_4$ are observed on top of the PS. Only the 30 min PS was used for bomb calorimetry, with the mass of samples used for the experiments varying from 19.05 to 64.11 ± 0.01 mg ($1.4-4.6 \times 10^{-3}$ moles Si). Once dry, the samples are sealed in the calorimeter bomb (Parr Instruments 1109A) and tested in a combustion calorimeter (Parr Instruments 6725) using a nickel-chrome fuse wire (Parr Instruments 45C10) for ignition. The ignition of 60 min samples was found to be very sensitive to friction, and since the fuse wire of the bomb calorimeter must physically contact the sample prior to ignition, the samples were too unstable for bomb calorimetric analysis. However, the 30 and 60 min samples could be used for DSC (TA Instruments 2920) analysis. The mass of

PS samples for DSC ranged from 0.52−0.69 ± 0.01 mg ($1.9-2.5 \times 10^{-5}$ moles Si) and 0.60−1.17 ± 0.01 mg ($2.2-3.9 \times 10^{-5}$ moles Si) for 30 and 60 min PS, respectively.

Heats of reaction are estimated from standard heats of formation where the reaction most likely follows eq 3. As a reference, according to eq 4, 32.5 kJ/g are liberated when Si reacts with just O_2.

$$2Si + NaClO_4 \rightarrow 2SiO_2 + 2NaCl \text{ (33.0 kJ/g Si)} \qquad (3)$$

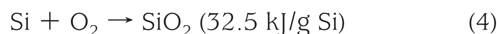

$$Si + O_2 \rightarrow SiO_2 \text{ (32.5 kJ/g Si)} \qquad (4)$$

For consistency, the computed heat of the reaction is given in terms of grams of Si only. There is a challenge in determining the mass of $NaClO_4$ oxidizer inside the PS because it tends to coat the surface of the PS and crystallize outside the pores. Since the material is very friction sensitive, the exposed oxidizer is difficult to physically remove without unintentionally igniting the PS sample. Further, cleaving the sample to view the $NaClO_4$ within the pores in cross-section would result in sample ignition. However, an upper limit for $NaClO_4$ loading in the pores is found by gravimetric analysis of PS-$NaClO_4$ samples used for DSC. This analysis indicates a 0.087 to 0.303 and 0.109 to 0.125 molar ratio of $NaClO_4$ to Si for 30 and 60 min PS, respectively. Equation 3 requires a molar ratio of 0.5 $NaClO_4$ to Si for complete oxidation of all of the PS, thus indicating that the expected experimental heat of reaction will range from 17−61% of theory. It is stressed though that some of this $NaClO_4$ mass may reside on top of the PS film and not actually be contained inside the pores where it most likely reacts with Si.

PS is organophillic such that the MeOH-$NaClO_4$ solution is drawn into the pores and it is assumed for the spongelike network of pores that it is loaded uniformly. The simple model in Figure 2a demonstrates the theoretical capacity of a PS film to contain $NaClO_4$. With the assumptions that all of the empty space in the pores is filled by $NaClO_4$ and that all of the $NaClO_4$ is able to react with all of the Si, the molar ratio of fuel to oxidizer can be computed using the density and molecular weight of Si and $NaClO_4$. The relationship between porosity and maximum molar ratio is plotted as the solid line in Figure 2a. The curve shows that the minimum porosity required to achieve the 0.5 molar ratio necessary for complete combustion is 68%, which is near the porosity of the 30 and 60 min PS. The experimental molar ratios lie below the theoretical capacity, however, indicating the porous structure is not completely filled by $NaClO_4$.

The bomb calorimetry data in Figure 2b confirms that the PS combustion reaction is most likely fuel-rich (i.e., Si-rich). When the calorimeter bomb is filled with either nitrogen or with dry air at atmospheric pressure the heat of the reaction, ΔH, is 10.8 ± 2.1 kJ/g of PS and 9.9 ± 1.8 kJ/g of PS respectively, well below the theoretical energy density. To confirm that the reaction is fuel rich, the bomb was filled with ~20 psig of O_2 ($\sim 1.2 \times 10^{-3}$ moles), which is slightly

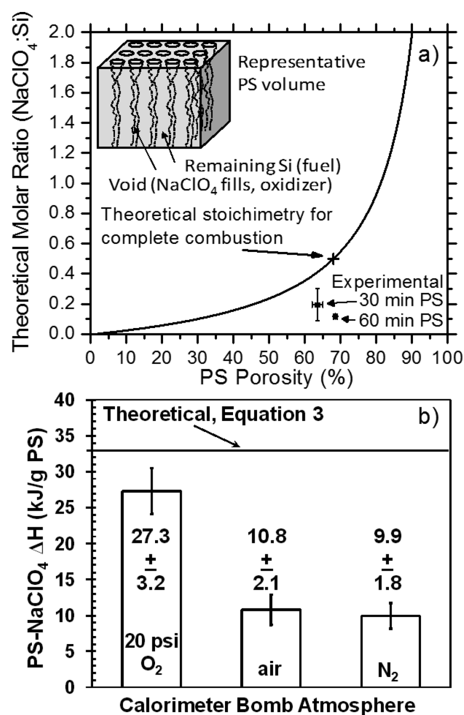

FIGURE 2. (a) Solid line represents the theoretical capacity of PS for $NaClO_4$ assuming all void space is filled with $NaClO_4$. Experimental and theoretical data for the stoichiometry are also shown. Inset: Schematic showing an idealized PS structure filled with oxidizer. (b) Bomb calorimetry results for 30 min PS. The theoretical heat of reaction corresponding to eq 3) is also given. All values are in terms of grams of PS and error bars represent the standard deviation of triplicate measurements.

less O_2 than is theoretically needed to react with all the PS, but a low enough pressure to not spontaneously ignite the sample (**note**: *high-pressure O_2 at ~400 psig will spontaneously ignite the sample, and care should be taken when working with O_2 and energetic PS*). In this case, the heat of reaction increases to 27.3 ± 3.2 kJ/g of PS, which is near the theoretical limit of 33 kJ/g of PS (eq 3) if all of the Si atoms in the PS network are oxidized. This indicates that the explosive reaction reaches temperatures such that oxidation by O_2 diffusion into the nanoscale Si domains of PS is possible, providing enough O_2 is present.

DSC has been employed in the study of PS and amorphous Si primarily to investigate oxidation and hydrogen desorption (19, 20). Here DSC is used to provide insight into PS oxidation, hydrogen desorption, and $NaClO_4$ decomposition in the context of our composite energetic material. Figure 3a shows DSC traces that demonstrate an explosion of PS-$NaClO_4$ in N_2 (as evidenced by a shattered chip in the high-pressure stainless steel DSC pan) releasing 6.1 ± 0.1 kJ/g of PS and initiating near 133 °C. The ΔH determined from DSC may be lower than that of bomb calorimetry due to the nature of the measurement which requires material to be in contact with the bottom of the DSC pan. During an explosion, this is not possible and some heat may be lost to the surroundings of the DSC sample compartment. Additionally, the observed decrease in molar ratio of $NaClO_4$ to Si in the 60 min sample would result in a decreased ΔH.

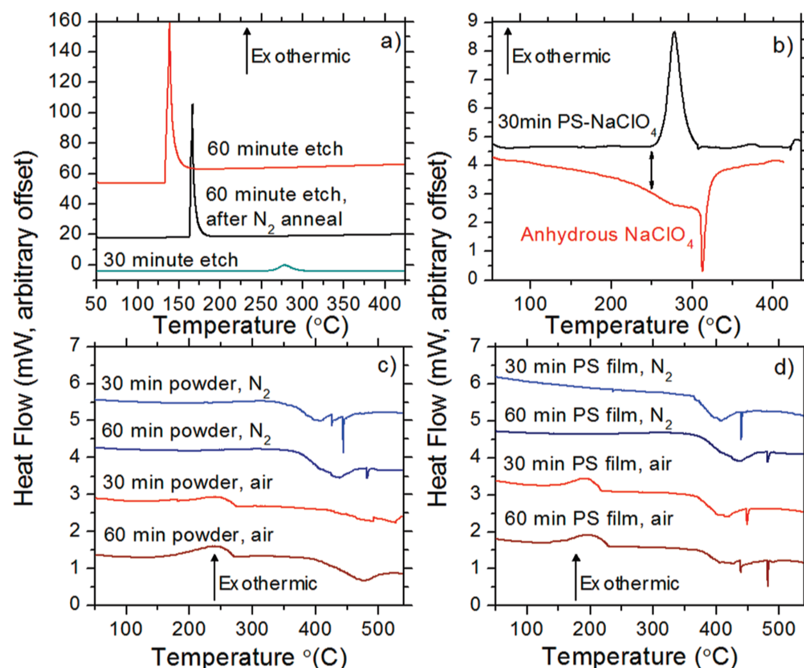

FIGURE 3. DSC scans (of absolute heat flow) of PS-$NaClO_4$, $NaClO_4$, PS powder, and PS films (10 °C/min) (a) 60 and 30 min PS-$NaClO_4$ in N_2, and 60 min PS-$NaClO_4$ after the PS had been subjected to heat treatment up to 450 °C in N_2. (b) $NaClO_4$ and 30 min PS-$NaClO_4$, the arrow indicates the endothermic peak of $NaClO_4$ initiates at the same temperature as the exothermic peak of PS-$NaClO_4$. (c) 60 and 30 min PS powders in air and N_2 (d) 60 and 30 min PS films on Si substrate in air and nitrogen.

The 30 min PS sample does not react explosively in the DSC (although it does explode when an intense heat pulse is used as in the bomb calorimetry fuse wire) and does not react until 264 °C releasing 1.0 ± 0.1 kJ/g of PS. This oxidation event is likely backbond oxidation of Si (19), and the source of the oxygen must come from partial decomposition of $NaClO_4$. While the exact mechanism of decomposition is not known, it is noted that p-type semiconductors facilitate sodium chlorate ($NaClO_3$) decomposition by accepting an electron, and a similar mechanism may apply here (21). Additionally, a scan of the 60 min PS-$NaClO_4$ is shown after the PS is heat treated in N_2 up to 450 °C (prior to applying the $NaClO_4$), and demonstrates that the explosive reaction occurs near 162 °C. Figure 3b shows DSC data of $NaClO_4$ only and the 30 min PS-$NaClO_4$. The $NaClO_4$ has an endothermic peak around 312 °C that is associated with the orthorhombic to cubic phase transition and a shoulder near 250 °C that coincides with the exothermic peak of the 30 min PS-$NaClO_4$ sample (22).

Panels c and d in Figure 3 show DSC scans of PS powder and PS films on Si substrates without $NaClO_4$. The scans are run in either air or N_2. PS powder was prepared by scraping the PS film from the substrate with a razor blade. For a given atmosphere, PS powder and thin films behave very similarly, indicating thickness of the PS film does not hinder its ability to react. Because the first peak is absent in scans in N_2, this peak is clearly associated with oxidation (most likely backbond oxidation of Si$-$H$_x$ (19)) and begins very near where the PS-$NaClO_4$ explosion begins. The endothermic peaks initiating near 350 °C are associated with hydrogen desorption (23, 24). Scanning the same sample twice results in a flat profile (not shown), indicating that the material has completely reacted during the initial scan.

Dropcasting $NaClO_4$ in MeOH onto PS results in variation of the $NaClO_4$:Si ratio as indicated earlier. Additionally, even lower molar ratios are realized by dropcasting a low molarity (0.2 M) $NaClO_4$-MeOH solution. Figure 4a shows DSC scans of 30 min PS-$NaClO_4$ to higher temperatures than in Figure 3a. Here the backbond oxidation peak is seen along with the thermal oxidation peak of Si that yields SiO_2 (19). The backbond oxidation peak is similar for 0.303 and 0.122 molar ratios but is reduced by roughly half and shifted to a lower temperature as the molar ratio drops to 0.02. Additionally, a scan of the decomposition of anhydrous $NaClO_4$ is shown where the endothermic peak near 480 °C represents melting and is followed by an exothermic peak representing decomposition (22, 25). Figure 4b explicitly shows that thermal oxidation does not occur until after hydrogen desorption. It is also noted that for this oxidation mechanism to progress, $NaClO_4$ must decompose, and in PS this decomposition actually occurs slightly before the melting point of $NaClO_4$, indicating the PS serves as a catalyst for $NaClO_4$ decomposition.

To verify the DSC results, we used Fourier transform infrared spectroscopy (FT-IR) to evaluate the surface termination of PS as a result of heat treatments and inclusion of $NaClO_4$. Figure 5a (30 min PS) shows that fresh PS and PS that has been dried with $NaClO_4$ and then rinsed with MeOH to remove the $NaClO_4$ are nearly identical. Both show very little O$-$Si$-$O bond character. This indicates that as a result of the hydrogen termination $NaClO_4$ does not partially oxidize the PS during drop-casting and therefore does not decrease the amount of available fuel for the reaction. For a heat treatment up to 250 °C in dry O_2, the Si$-$H$_x$ still remains but O$-$Si$-$O has become much more pronounced and small backbond oxidation peaks appear from 2150$-$2300

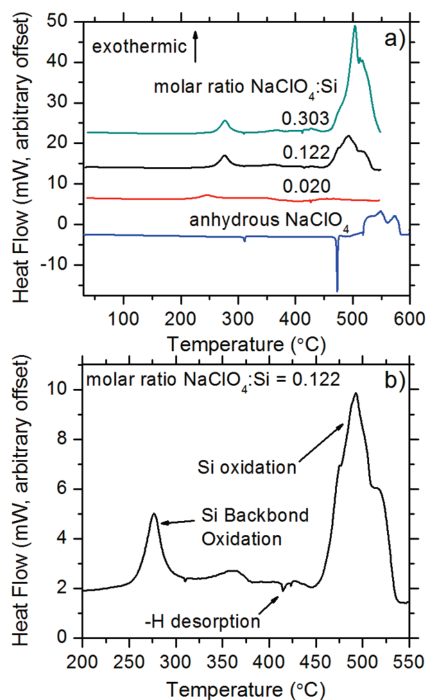

FIGURE 4. DSC scans of 30 min PS-$NaClO_4$ and $NaClO_4$ (10 °C/min) (a) Increase of SiO_2 oxidation peak with increasing molar ratio of $NaClO_4$:Si. Compared to pure $NaClO_4$, the decomposition of $NaClO_4$ in PS occurs slightly below the $NaClO_4$ melting point rather than after the melting point. (b) Enhanced view of the 0.122 molar ratio peak from a showing the backbond oxidation peak, hydrogen desorption, and Si oxidation.

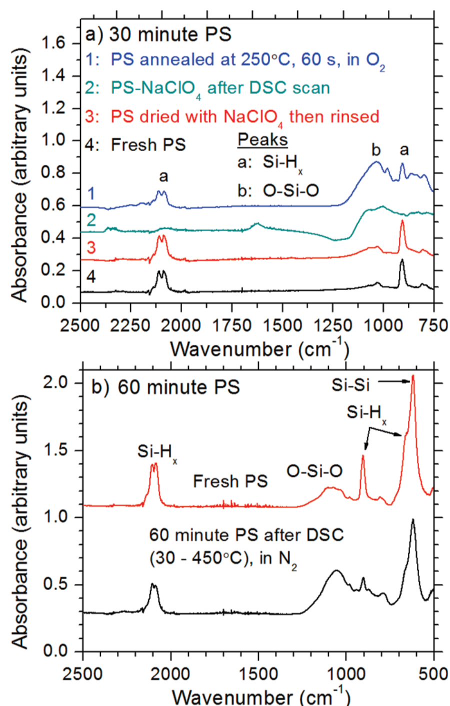

FIGURE 5. (a) Fourier transform infrared spectroscopy (FTIR) of 30 min PS. Curve 1 shows the PS after a mild anneal of 250 °C in O_2 for 60s, curve 2 shows the PS-$NaClO_4$ after the DSC run, curve 3 shows PS that had $NaClO_4$ fill the pores but then was rinsed with MeOH, and curve 4 shows fresh PS. (b) FTIR of fresh 60 min PS and 60 min PS after a DSC scan from 30−450 °C in N_2.

cm^{-1} (19). This confirms the DSC result that the oxidation peak seen with $NaClO_4$ near 250 °C involves backbond oxidation. Additionally, curve 2 shows the 30 min PS-$NaClO_4$ after a DSC run to 450 °C (below the temperature for complete hydrogen desorption) and exhibits minor contributions of Si−H_x bonding but primarily O−Si−O, which gives rise to the exothermic signal in DSC. The peaks near 2345 and 1626 cm^{-1} correspond to CO_2 and H_2O respectively, where the H_2O likely results from the hygroscopic nature of residual $NaClO_4$ on the PS surface. Figure 5b (60 min PS) shows that in N_2 even up to 450 °C, the Si−H_x bond remains as indicated by the peaks near 2100 and 910 cm^{-1} and the shoulder at 660 cm^{-1} on the Si−Si peak at 620 cm^{-1} (24). The O−Si−O peak does increase somewhat, indicating a small amount of O_2 was present during heating. For the heat treatments mentioned in N_2 or O_2, PS is still capable of explosion by mechanical impact or initiator wire.

The FT-IR and DSC data suggest that PS-$NaClO_4$ can only produce an explosion if hydrogen termination is present at the time of initiation. FT-IR reveals that Si−H_x remains up to 450 °C, well above the ignition temperature for PS-$NaClO_4$. Additionally, the O−Si−O bonding does increase after heat treatment of PS in oxygen at 250 °C and DSC reveals that oxidation begins approximately at the same temperature at which the 60 min PS-$NaClO_4$ ignites. Because the 30 min PS-$NaClO_4$ remains inert until just above 250 °C, backbond oxidation is likely not serving as the ignition source. As suggested by Kovalev et al. (26), one possibility is that the reaction is triggered by exposure of a Si radical as might occur during cracking of the PS structure. Until this crack occurs from thermal stress or mechanical impact, the hydrogen termination prevents Si oxidation. The 60 min PS structure is more fragile (as evidenced by cracks on the surface after etching) than the 30 min PS structure and is therefore more susceptible to cracking from thermal stress, which likely explains why only the 60 min sample explodes during the slow heating rate of the DSC scan. A locally occurring oxidation resulting from Si radical bonds reacting with $NaClO_4$ produces enough heat to initiate a chain reaction which heats rapidly to remove hydrogen and then oxidizes Si. This result yields H_2 gas that is likely a contributor to the large flames and pressures observed during PS-$NaClO_4$ explosions.

In summary, we have used a galvanic corrosion route to PS formation that yields PS layers thicker than 150 μm without the need for a power supply or custom etch cell. We show bomb calorimetry and DSC results of the galvanic PS material reacting with $NaClO_4$ oxidizer. These results confirm that the dropcasting of $NaClO_4$ into PS yields a fuel-rich material capable of yielding 9.9 ± 1.8 kJ/g of PS when reacted in N_2. However, this reaction reaches sufficient temperature such that if gaseous O_2 is also present, all of the Si atoms in the PS are oxidized and the theoretical heat of reaction of PS-$NaClO_4$ is nearly achieved, producing 27.3 ± 3.2 kJ/g of PS. Finally, with DSC and FT-IR analysis, the initiation temperature of PS-$NaClO_4$ is found to be as low as 133 °C, whereas Si−H_x bonds on the PS surface are stable up to 450 °C. If hydrogen is desorbed from the PS film, an explosion does not occur despite a large heat of reaction from Si oxidation. If

hydrogen is present, and the PS-$NaClO_4$ is triggered with a rapid heating initiator wire or mechanical impact, the composite reacts explosively. These results highlight the unique role of the hydrogen termination of PS that ultimately facilitates the explosive reaction of PS-$NaClO_4$.

Acknowledgment. Collin Becker is funded by a Department of Defense SMART fellowship and is grateful to the U.S. Army Research Lab for hosting his research. Funding for galvanic PS research was provided under U.S. Army Research Office grant no. W911NF-06-1-0342. The authors thank Dr. Brian Larsen, Dr. David Miller, and Brendan Hanrahan for beneficial discussions.

REFERENCES AND NOTES

(1) Canham, L., Ed. *Properties of Porous Silicon; INSPEC*; The Institution of Electrical Engineers: London, 1997.
(2) Mikulec, F. V.; Kirtland, J. D.; Sailor, M. J. *Adv. Mater.* **2002**, *14*, 38–41.
(3) Clement, D.; Diener, J.; Gross, E.; Kunzner, N.; Timoshenko, V. Y.; Kovalev, D. *Phys. Status Solidi A* **2005**, *202*, 1357–1364.
(4) Currano, L. J.; Churaman, W. A. *J. Microelectromech.* **2009**, *18*, 799–807.
(5) Du Plessis, M. *Phys. Status Solidi A* **2007**, *204*, 2319–2328.
(6) Churaman, W. A.; Currano, L. J.; Becker, C. R. *J. Phys. Chem. Solids* **2010**, *71*, 69–74.
(7) Ashruf, C. M. A.; French, P. J.; Bressers, P.; Kelly, J. J. *Sens. Actuators, A* **1999**, *74*, 118–122.
(8) Kelly, J. J.; Xia, X. H.; Ashruf, C. M. A.; French, P. J. *IEEE Sens. J.* **2001**, *1*, 127–142.
(9) Miller, D. C.; Boyce, B. L.; Gall, K.; Stoldt, C. R. *Appl. Phys. Lett.* **2007**, *90*, 191902.
(10) Miller, D. C.; Becker, C. R.; Stoldt, C. R. *J. Electrochem. Soc.* **2008**, *155*, F253–F265.
(11) Pierron, O. N.; Macdonald, D. D.; Muhlstein, C. L. *Appl. Phys. Lett.* **2005**, *86*, 211919.
(12) Splinter, A.; Sturmann, J.; Benecke, W. *Sens. Actuators, A* **2001**, *92*, 394–399.
(13) Becker, C. R.; Miller, D. C.; Stoldt, C. R. *J. Micromech. Microeng.* **2010**, *20*, 085017.
(14) Pant, A. K.; Murarka, S. P.; Shepard, C.; Lanford, W. *J. Appl. Phys.* **1992**, *72*, 1833–1836.
(15) Barrett, E. P.; Joyner, L. G.; Halenda, P. P. *J. Am. Chem. Soc.* **1951**, *73*, 373–380.
(16) Bomchil, G.; Herino, R.; Barla, K.; Pfister, J. C. *J. Electrochem. Soc.* **1983**, *130*, 1611–1614.
(17) Herino, R.; Bomchil, G.; Barla, K.; Bertrand, C.; Ginoux, J. L. *J. Electrochem. Soc.* **1987**, *134*, 1994–2000.
(18) Ruike, M.; Houzouji, M.; Motohashi, A.; Murase, N.; Kinoshita, A.; Kaneko, K. *Langmuir* **1996**, *12*, 4828–4831.
(19) Salonen, J.; Lehto, V. P.; Laine, E. *Appl. Phys. Lett.* **1997**, *70*, 637–639.
(20) Roura, P.; Farjas, J.; Cabarrocas, P. R. I. *Thin Solid Films* **2009**, *517*, 6239–6242.
(21) Wydeven, T. *J. Catal.* **1970**, *19*, 162.
(22) Devlin, D. J.; Herley, P. J. *React. Solids* **1987**, *3*, 75–84.
(23) Salonen, J.; Lehto, V. P.; Laine, E. *J. Porous Mater.* **2000**, *7*, 335–338.
(24) Gupta, P.; Colvin, V. L.; George, S. M. *Phys. Rev. B* **1988**, *37*, 8234–8243.
(25) Shimada, S. *Thermochim. Acta* **1992**, *196*, 237–246.
(26) Kovalev, D.; Timoshenko, V. Y.; Kunzner, N.; Gross, E.; Koch, F. *Phys. Rev. Lett.* **2001**, *87*.

AM100975U